Journal of Fluids and Structures 17 (2003) 643–664

JOURNAL OF FLUIDS AND STRUCTURES

www.elsevier.nl/locate/jnlabr/yjfls

Hydrodynamic loads during water entry of two-dimensional and axisymmetric bodies

D. Battistin, A. Iafrati*

INSEAN, Istituto Nazionale per Studi ed Esperienze di Architettura Navale, Via di Vallerano, 139, 00128 Roma, Italy

Received 20 December 2001; accepted 27 November 2002

Abstract

In this paper the free-surface flow generated by the vertical water entry of two-dimensional symmetric and axisymmetric bodies of arbitrary shape is numerically investigated. The study is carried out in the framework of potential flow of an incompressible fluid with gravity and surface tension effects also neglected. The unsteady flow is computed through a boundary-element formulation and nonlinearities in the free-surface boundary conditions are fully retained. Attention is mainly focused on evaluating the pressure distribution and the total hydrodynamic load acting on the impacting body. For validation, the approach is applied to the water impact of a cone with constant entry velocity, and checks of the self-similarity of the solution are made. Next, the water impact of a circular cylinder and of a sphere are analyzed. Comparisons with available theoretical solutions and experimental data are made.

1. Introduction

In this paper, the water impact of two-dimensional and axisymmetric bodies is numerically investigated and the corresponding pressure field and total hydrodynamic load acting on the body contour are carefully evaluated. The numerical procedure has been largely validated in the past for the impact of two-dimensional wedges both in the case of constant entry velocity and free drop. Here the approach is extended to bodies having arbitrary and, presumably, more realistic shapes.

The prediction of the hydrodynamic loads acting on the wetted part of an impacting body is very important in the naval field both for structural design and for the prediction of some seakeeping properties of the ship. However, slamming load prediction is not the only case in which fluid dynamics of water entry is of some importance in the naval context. Actually, the free-surface flow taking place in transverse planes about high-speed planing craft has strong similarities with that generated during water impact. This aspect is exploited by the so-called $2D + t$ approach and studies in this direction have been carried out by Zhao et al. (1997), Savander (1997) and Xu and Troesh (1999), among others.

The description of the fluid flow about bodies impacting the free surface is made difficult by the flow singularity that occurs about the intersection of the body contour with the free surface and which, for small deadrise angles, gives rise to a high-pressure peak localized at the spray root. Furthermore, in the impact of bodies having convex contours or sudden increment of the deadrise angle, the jet flow can detach from the body contour, thus making the investigation of the resulting fluid flow even more complex (Greenhow, 1987,1988). A model that significantly simplifies the numerical description of the jet flow has been proposed by Zhao and Faltinsen (1993) and a similar approach has been adopted in Iafrati et al. (2000) to describe the flow about two-dimensional wedges impacting the free surface. In Zhao et al. (1996)

*Corresponding author. Tel.: +39-06-50299296; fax: +39-06-5070619.
E-mail address: a.iafrati@insean.it (A. Iafrati).

0889-9746/03/$ - see front matter
doi:10.1016/S0889-9746(03)00010-0

the same model has been used to study the flow about bodies having arbitrary contours, and it has been extended to deal with the flow separation for geometries where the detachment point can be easily recognized, like hard chines in planing hulls.

In this paper the flow generated by the impact of a cylinder and a sphere is numerically investigated, and comparisons with available experimental data and theoretical solutions are conducted. The entry velocity is assumed to be vertical and the body symmetric with respect to the vertical axis, thus always resulting in symmetric flow conditions. The study is carried out within the hypotheses of irrotational flow of an inviscid and incompressible fluid with negligible gravity and surface tension effects. Consistent with these assumptions, a velocity potential is introduced and its boundary integral representation is employed within the fluid domain. A Neumann condition is applied on the wetted part of the body contour and a Dirichlet condition is applied on the free surface. By using the kinematic and dynamic conditions, the velocity potential on the free surface is obtained by integrating in time the unsteady Bernoulli equation. For the sake of limiting the computational effort, the thin jet developing about the intersection of the free surface with the body is cut off the computational domain and it is replaced by a straight panel orthogonal to the solid boundary with a suitable boundary condition applied there.

As aforementioned the numerical approach has previously been validated in the case of a two-dimensional wedge impacting the free surface (Iafrati et al., 2000). In the following, the same model is first extended to deal with axisymmetric bodies and, for validation, the water impact of a cone with constant entry velocity is computed, recovering the self-similar behavior which is compared with the fully nonlinear theoretical solution given by Schiffman and Spencer (1951) and with the asymptotic estimate (Faltinsen and Zhao, 1997). Next, the two-dimensional approach is extended to deal with bodies having arbitrary sections and the flow about a circular cylinder entering the water surface with a constant entry velocity is studied. Results are compared with the experimental data of Campbell and Weynberg (1980) and with the asymptotic estimate by Cointe and Armand (1987). Finally, the flow about a sphere is studied, and comparisons are made with the asymptotic solutions by Miloh (1991) and Faltinsen and Zhao (1997) and with the experimental data of Moghisi and Squire (1981), Baldwin and Steves (1975) and Nisewanger (1961).

2. Formulation of the problem

The vertical water entry of two-dimensional symmetric and axisymmetric bodies onto an initially undisturbed water surface is here investigated. The fluid domain Ω is assumed to be unbounded in the horizontal direction and infinitely deep. Owing to symmetry, the study is carried out on the right half of a plane (y, z), where z is the vertical axis oriented upwards with $z = 0$ on the still water level, and y is the horizontal axis oriented from left to right with $y = 0$ at the symmetry axis. With this notation, the fluid is bounded by the free surface S_F on the top and by the body contour S_B on the left (Fig. 1). At this stage of the study, the water entry velocity $\boldsymbol{w} = -U\boldsymbol{e}_z$ is assumed to be constant during the impact, $\boldsymbol{e}_z$ being the unit vector directed along the z-axis.

The fluid is approximated as ideal and incompressible with negligible surface tension effects. Gravity effects can be also neglected as long as $gt/U \ll 1$, that is during the early stage of the impact. By assuming the flow to be irrotational, it may be described in terms of the velocity potential ϕ which satisfies the Laplace equation inside the fluid domain, the impermeability constraint on the body contour and the dynamic and kinematic boundary conditions on the free surface, that is

$$\nabla^2\phi = 0 \quad (\Omega), \tag{1}$$

$$\frac{\partial\phi}{\partial n} = \boldsymbol{w}\cdot\boldsymbol{n} = -Un_z \quad (S_B), \tag{2}$$

$$\frac{\mathrm{D}\phi}{\mathrm{D}t} = \frac{|\nabla\phi|^2}{2} \quad (S_F), \tag{3}$$

$$\frac{\mathrm{D}\boldsymbol{x}}{\mathrm{D}t} = \nabla\phi \quad (S_F), \tag{4}$$

where $\boldsymbol{n}$ is the unit vector normal to the surface oriented inwards. The form used to write the last two conditions highlights the mixed Eulerian–Lagrangian formulation which is adopted to numerically solve the initial–boundary-value problem (Longuet-Higgins and Cokelet, 1976).

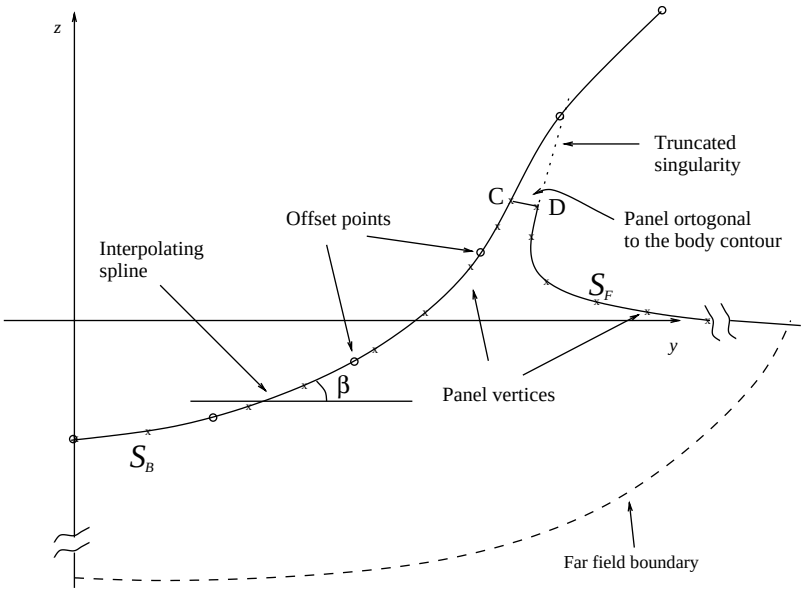

Fig. 1. Sketch of the discretization employed about the jet cut.

At each time step, the solution of the boundary-value problem for the velocity potential is sought in the form of the boundary integral representation provided by the second Green's identity

$$\phi(\boldsymbol{x}_P) = \int_{S_F \cup S_B \cup S_\infty} \left(\phi(\boldsymbol{x}_Q) \frac{\partial G(\boldsymbol{x}_P - \boldsymbol{x}_Q)}{\partial n_Q} - \frac{\partial \phi(\boldsymbol{x}_Q)}{\partial n_Q} G(\boldsymbol{x}_P - \boldsymbol{x}_Q) \right) \mathrm{d}S_Q \quad (\boldsymbol{x}_P \in \Omega), \tag{5}$$

where S_∞ is the boundary at infinity and $G(\boldsymbol{x}_P - \boldsymbol{x}_Q)$ is the free-space Green's function of the Laplace operator which is

$$G(\boldsymbol{x}_P - \boldsymbol{x}_Q) = \frac{1}{2\pi} \log(|\boldsymbol{x}_P - \boldsymbol{x}_Q|)$$

in two dimensions and

$$G(\boldsymbol{x}_P - \boldsymbol{x}_Q) = -\frac{1}{4\pi |\boldsymbol{x}_P - \boldsymbol{x}_Q|}$$

in three dimensions.

According to the boundary-value problem stated by Eqs. (1)–(4), in the integral representation (5) the velocity potential is known on the free surface S_F, while its normal derivative is assigned on the body contour. In order to get the velocity potential along the body contour and its normal derivative along the free surface, the boundary integral representation (5) is written in the limit as $\boldsymbol{x}_P$ approaches the boundary of the fluid domain $\partial\Omega = S_F \cup S_B \cup S_\infty$, thus obtaining, for smooth contours,

$$\frac{1}{2} \phi(\boldsymbol{x}_P) = \int_{S_F \cup S_B \cup S_\infty} \left(\phi(\boldsymbol{x}_Q) \frac{\partial G(\boldsymbol{x}_P - \boldsymbol{x}_Q)}{\partial n_Q} - \frac{\partial \phi(\boldsymbol{x}_Q)}{\partial n_Q} G(\boldsymbol{x}_P - \boldsymbol{x}_Q) \right) \mathrm{d}S_Q \quad (\boldsymbol{x}_P \in \partial\Omega), \tag{6}$$

which leads to a boundary integral equation of mixed first and second kind. Once Eq. (6) is solved, the velocity potential and its normal derivative are known all along the body contour and the free surface, thus allowing one to determine the velocity potential inside the fluid domain through Eq. (5).

The solution of the boundary integral equation (6), providing the normal derivative of the velocity potential on S_F, allows the determination of the velocity field on the free surface. Then Eqs. (3) and (4) can be integrated in time through a two-step Runge–Kutta scheme to update the free-surface shape and the velocity potential on it.

A major issue for slamming and water-entry flows concerns the treatment of the velocity singularity that occurs at the intersection between the free surface and the body contour. As a starting configuration, it is assumed that a very small portion of the body is already submerged and the velocity potential is null throughout the undisturbed free surface. The velocity field associated with these boundary conditions is singular at the intersection point, and an accurate description of the corresponding starting flow would require a deeper investigation (Iafrati and Korobkin, 2001). It is worth

remarking that this singular behavior is a result of the assumptions made in the model: surface tension is important in a very small neighborhood of the jet tip while compressibility effects have a role in a very early stage after the impulsive start. However, both these effects do not significantly affects the overall impact dynamics.

As a consequence of the flow singularity at the intersection, a thin jet develops whose accurate description would require a quite intensive computational effort. Moreover, this jet, being very thin, has almost zero pressure, so that its contribution to the overall impact force is negligible. For this reason, the same approach suggested by Zhao and Faltinsen (1993) is used here, that is the jet is cut-off and replaced by a suitable boundary condition applied at the jet truncation. The model is discussed in more detail in Section 3.

2.1. Pressure distribution and hydrodynamic load

The pressure distribution along the body contour is obtained through the Bernoulli's equation:

$$p = -\rho\left(\frac{\partial\phi}{\partial t} + \frac{|\nabla\phi|^2}{2}\right), \tag{7}$$

ρ being the fluid density, and the total hydrodynamic load is obtained by integration of the pressure field along the wetted part of the body

$$\boldsymbol{F} = -\int_{S_B} p\boldsymbol{n}\,\mathrm{d}S. \tag{8}$$

To evaluate the pressure distribution along the body contour through Eq. (7), the time derivative of the velocity potential $\dot{\phi} \equiv \partial\phi/\partial t$ has to be provided. One way to get this quantity consists in evaluating the velocity potential at two different time instants and then in using the definition of the material derivative to recover $\dot{\phi}$, i.e.

$$\dot{\phi} = \frac{\mathrm{D}\phi}{\mathrm{D}t} - \boldsymbol{v}\cdot\nabla\phi, \tag{9}$$

where $\boldsymbol{v}$ is the velocity of the point considered. It is rather natural to choose the panel centroids as material points where the velocity potential and its normal derivative are known after the boundary integral Eq. (6) is solved. Unfortunately, this technique is prone to induce oscillations in the pressure field, either when the jet is cut-off or when the discretization on the body is changed from one step to another.

As an alternative, $\dot{\phi}$ can be directly evaluated by exploiting its harmonic properties throughout the fluid domain. Since in this approach only instantaneous flow conditions are involved, much more stable results are obtained (Battistin and Iafrati, 2001). The method is based on the use of an integral representation for $\dot{\phi}$, similar to Eq. (5), and on the solution of another boundary integral equation with a Dirichlet condition on the free surface and a Neumann condition on the body contour, in the same way as it is done for ϕ.

The Dirichlet condition on the free surface is directly provided by the dynamic boundary condition (3) that reads

$$\dot{\phi} = -\frac{|\nabla\phi|^2}{2}(S_F), \tag{10}$$

while the evaluation of its normal derivative on the body contour needs some algebra to be recast in a form which can be easily computed from kinematic and geometric quantities available on the boundary of the fluid domain. Details of the derivation of $\partial\dot{\phi}/\partial n$ on the body contour are in Appendix A; only the final result is reported here. In the case of rigid bodies impacting the water surface with a constant heel angle, it can be shown that (Cointe, 1989; Wu and Eatock Taylor, 1996)

$$\frac{\partial\dot{\phi}}{\partial n} = \boldsymbol{n}\cdot\boldsymbol{a}_0 - \boldsymbol{n}\cdot(\boldsymbol{w}\cdot\nabla)\boldsymbol{u}, \tag{11}$$

where $\boldsymbol{a}_0$ is the body acceleration and $\boldsymbol{u} = \nabla\phi$ is the fluid velocity. For a constant entry velocity $\boldsymbol{w}$, the first term in Eq. (11) vanishes and the second contribution could be evaluated by taking the normal derivative of the velocity field. From a numerical standpoint, computing the normal derivative of the velocity field at the boundary is not reliable and it is even strongly dependent on the discretization employed (Tanizawa, 1995). To overcome this difficulty, the term $\boldsymbol{n}\cdot(\boldsymbol{w}\cdot\nabla)\boldsymbol{u}$ is rearranged as a combination of tangential derivatives by using the continuity equation. In doing that, the parametric description of the body as an axisymmetric one is used

$$\boldsymbol{x}_P(\theta, s) = (r(s)\cos\theta, r(s)\sin\theta, z(s)), \tag{12}$$

where θ is the azimuthal angle (the two-dimensional problem is recovered for $\theta = \pi/2$) and s is the natural parameter along the meridian contour, that is $(r')^2 + (z')^2 = 1$, where prime denotes differentiation with respect to s. As shown in

the Appendix, the term $\boldsymbol{n}\cdot(\boldsymbol{w}\cdot\boldsymbol{\nabla})\boldsymbol{u}$ is reduced as follows:

$$\boldsymbol{n}\cdot(\boldsymbol{w}\cdot\boldsymbol{\nabla})\boldsymbol{u} = w_s\partial_s u_n - w_n\partial_s u_s + k_{sn}w_s u_s + (k_{sn}+k_{\theta n})w_n u_n - \frac{r'}{r}w_n u_s, \tag{13}$$

where $\partial_{s,n}$ denote spatial differentiation with respect to s and n, respectively, and $k_{sn}, k_{\theta n}$ are the normal curvatures of the two coordinate lines. In Eq. (13), $\{u_s, u_n\}$ are the projection of the fluid velocity, which lies in the meridian plane since the flow is swirl-free, along the tangent and the normal to the body contour, respectively. In two-dimensions Eq. (13) can be further simplified, as shown in Appendix A, by removing the terms related to the azimuthal variable, thus obtaining

$$\boldsymbol{n}\cdot(\boldsymbol{w}\cdot\boldsymbol{\nabla})\boldsymbol{u} = w_s\partial_s u_n - w_n\partial_s u_s + k_s\boldsymbol{w}\cdot\boldsymbol{u}. \tag{14}$$

3. Description of the numerical approach

The solution of the initial–boundary-value problem is achieved via a mixed Eulerian–Lagrangian formulation based on a boundary element approach, zero-order accurate in space, and on a two-step Runge–Kutta scheme for time integration, as described below. When dealing with axisymmetric impact the solution is completely determined once variables are known in a meridian plane. Thus the numerical procedure is illustrated in the (y,z)-plane, the difference between two-dimensional and axisymmetric calculations only being in the different Green's functions used to evaluate the influence coefficients in Eqs. (5) and (6).

The body contour in the (y,z)-plane is provided in terms of a cubic spline representation through a given set of offsets. The wetted part of the body contour is then discretized with segments having their vertices located along the spline curve (Fig. 1). Along each panel both the velocity potential and its normal derivative are assumed to be constant and equal to the value they take at the centroid. When using this discretization in the boundary integral representation (5) or in the boundary integral equation (6), influence coefficients have to be evaluated as follows:

$$\begin{aligned} g_{ij} &= \int_{S_j} G(\boldsymbol{x}_{P_i} - \boldsymbol{x}_Q)\,\mathrm{d}S_Q, \\ dg_{ij} &= \int_{S_j} \frac{\partial G}{\partial n_Q}(\boldsymbol{x}_{P_i} - \boldsymbol{x}_Q)\,\mathrm{d}S_Q, \end{aligned} \tag{15}$$

where S_j denotes the portion of fluid boundary represented by the jth panel and $\boldsymbol{x}_{P_i}$ is the centroid of the ith panel, or, in the axisymmetric case, it is the center of the intersection of the panel with the meridian plane. In two dimensions coefficients (15) can be evaluated analytically while in the axisymmetric case the integration in the azimuthal direction is performed analytically, and then the integration along the meridian section of the panel is carried out numerically. By introducing the following notation:

$$\begin{aligned} &\boldsymbol{x}_{P_i} \equiv (y_i, 0, z_i), \quad \boldsymbol{x}_Q \equiv (y\cos\theta, y\sin\theta, z), \\ &\boldsymbol{n}_Q \equiv (\tilde{n}\cos\theta, \tilde{n}\sin\theta, n_z), \\ &\delta^2 \equiv (y_i - y)^2 + (z_i - z)^2, \\ &h^2 \equiv \frac{4y_i y}{\delta^2 + 4y_i y}, \end{aligned}$$

$\tilde{n}$ denoting the amplitude of the projection of the normal vector $\boldsymbol{n}$ onto the horizontal plane, the influence coefficients g_{ij} and dg_{ij} in the axisymmetric case can be rewritten as follows:

$$g_{ij} = -\frac{1}{\pi}\int_0^{l_j} \frac{y}{\sqrt{\delta^2 + 4y_i y}} F(h)\,\mathrm{d}\xi, \tag{16}$$

$$\begin{aligned} dg_{ij} = -\frac{1}{\pi}\int_0^{l_j} \frac{y}{\sqrt{(\delta^2 + 4y_i y)^3}} \Bigg[&\tilde{n}y_i\left(E(h)\frac{1}{1-h^2}\left(\frac{2}{h^2} - 1\right) - \frac{2}{h^2}F(h)\right) \\ &- \tilde{n}y\frac{E(h)}{1-h^2} + n_z(z_i - z)\frac{E(h)}{1-h^2}\Bigg]\,\mathrm{d}\xi, \end{aligned} \tag{17}$$

where ξ is the parameter along the intersection of the jth panel with the (y,z) plane, l_j is its length and

$$F(h)=\int_0^{\pi/2}\frac{\mathrm{d}\alpha}{\sqrt{1-h^2\cos^2\alpha}},\quad E(h)=\int_0^{\pi/2}\sqrt{1-h^2\cos^2\alpha}\,\mathrm{d}\alpha$$

are the *first* and *second complete elliptic integrals* (Gradshteyn and Ryzhik, 1980).

Due to the logarithmic singularity of the first complete elliptic integral, both the integrands of the influence coefficients g_{ij}, dg_{ij} diverge as $h\to 1$, that is as $\boldsymbol{x}_Q\to\boldsymbol{x}_{P_i}$, but their integrals are finite. The use of a Gauss formula with an even number of points allows an accurate evaluation of the integrals: convergence tests showed that eight Gauss points are enough to provide accurate results throughout all simulations.

When writing the boundary integral representation (5) in discrete form, the contributions from the far field boundary S_∞ can be neglected as long as the domain extension is large enough. As already stated, the solution of the boundary integral equation (6) gives back the distributions of the velocity potential on the body contour and its normal derivative on the free surface, thus allowing the computation of the velocity field all along the free surface. This latter is used to move free-surface centroids by using Eq. (4), which is integrated in time by means of a two-step Runge–Kutta scheme. For stability reasons, the time step is chosen such that the maximum displacement of each centroid is always smaller than one fourth of the corresponding panel length. The dynamic boundary condition (3) is also integrated in time to update the distribution of the velocity potential on the free surface.

Once the location of the panel centroids at the new time step is recovered, a cubic spline through them is used and the distribution of panel vertices and centroids is reinitialized. It is important to remark that, although the boundary integral equation (6) is collocated at the panel midpoints, Lagrangian points used to track the free-surface motion are always located along the spline curve, thus resulting in better mass conservation properties (Zhao and Faltinsen, 1993). At the reconstruction stage suitable constraints are enforced to keep a good accuracy. Redistribution is started at the jet tip where the length of the first free-surface panel is assigned to be equal to the distance from the body contour. Starting from this value, a growth factor for the panel length is applied but, to preserve the accuracy in describing highly curved regions, the length is fixed so that the angle between adjacent panels is always less than a maximum fixed value. The discretization of the body contour is updated in a similar way by using the same length for the panel closest to the jet tip and the same growth factor.

The main point in developing the numerical approach concerns the treatment of the flow singularity that takes place at the intersection point, since the description of the resulting thin jet would require an extremely refined discretization. To avoid this, some models (Zhao and Faltinsen, 1993; Fontaine and Cointe, 1997) have been developed which cut-off the jet and replace it with a suitable boundary condition at the truncation. This approximation is motivated by the rather negligible contribution given by the jet to the impact loads, in spite of the not negligible kinetic energy associated with it (see for instance Molin et al., 1996; Faltinsen et al., 1999). The reason is that only weak variations of the pressure field occur inside this region, thus resulting in an almost atmospheric pressure value on the part of the body contour wetted by the jet.

The model here employed is similar to that suggested by Zhao and Faltinsen (1993) and the present implementation of it has been thoroughly validated both in the constant entry velocity case and in the free fall of two-dimensional wedges (Iafrati et al., 2000). In a first stage the free surface is assumed to touch the body, which is slightly submerged in its initial configuration (see Fig. 2). Due to the velocity singularity at the intersection, a thin jet develops, characterized by a strong velocity gradient normal to the body contour. When the distance between the body and the first centroid on the free surface becomes smaller than a fixed threshold value, the jet is cut-off the computational domain and it is

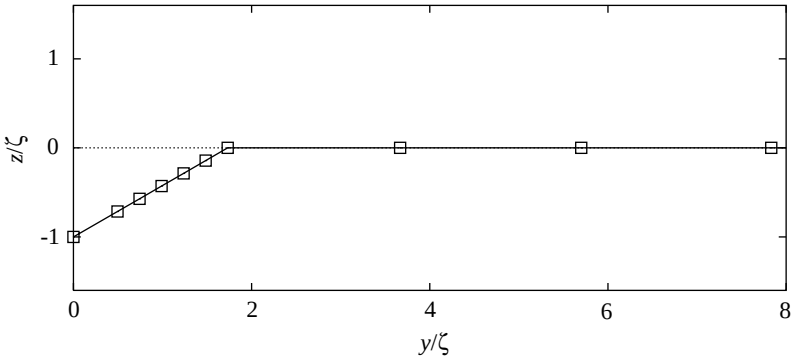

Fig. 2. Close-up view of the initial discretization used about the intersection point for the impact of a cone with 30° deadrise angle.

replaced by a panel normal to the body contour which passes through the first panel vertex on the free surface (Fig. 1). On this new panel both the velocity potential and its normal derivative are supposed unknown, thus an additional equation is introduced by requiring that the normal velocity on the panel is equal to the value that is extrapolated from the velocity field on the free surface. After the first cut, the angle between the first free-surface panel and the body contour is monitored and when it becomes smaller than a fixed value a new cut is made. The limiting value of the angle is chosen at the beginning of the simulation and it is usually between 4° and 10°, depending on the body shape, with smaller values used for flatter geometries.

4. Numerical results

The proposed numerical approach has been extensively validated in Iafrati et al. (2000) for the impact of two-dimensional wedges. A detailed investigation of the role of the parameters governing the cut was performed and the results in terms of the total hydrodynamic force proved to be rather insensitive to the precise details of the jet treatment.

In the present paper attention is mainly focused on the extension of the numerical approach to axisymmetric bodies and to arbitrary shapes. The numerical procedure is first extended to deal with axisymmetric bodies and then it is validated in the case of an impacting cone with 30° deadrise angle. Results are compared with the theoretical solution by Schiffman and Spencer (1951) and with the asymptotic theory (Faltinsen and Zhao, 1997). Next, it is extended to arbitrary geometry and validated in the case of a circular cylinder, for which comparisons are made with the experimental data of Campbell and Weynberg (1980) and with the asymptotic estimate by Cointe and Armand (1987). Finally the flow generated by the impact of a sphere is analyzed and results are compared with the asymptotic solutions given by Miloh (1991) and by Faltinsen and Zhao (1997), and with the experimental data of Baldwin and Steves (1975), Moghisi and Squire (1981) and Nisewanger (1961).

4.1. Cone

In order to validate the numerical approach and the axisymmetric formulation, the impact of a cone with constant entry velocity is studied. As in the corresponding wedge problem in two dimensions, the solution is self-similar, that is the solution is time independent in a suitable set of nondimensional variables. The numerical solution is started from a still free surface with the body already submerged, as shown in Fig. 2. In the following, $\zeta(t) = -z(y = 0)$ denotes the position of the apex of the body, with $\zeta(0)$ indicating the initial depth. Due to the symmetry of the flow, only the right-hand side of the fluid domain ($y \geqslant 0$) is considered in the numerical calculation. The computational domain extends from $y = 0$ to 800 $\zeta(0)$, and the length of the first panel closest to the body contour is 2 $\zeta(0)$. Six panels are used to discretize the initial wetted portion of the body contour.

During the early stage of the numerical calculation the thin jet develops (*turning phase*), and the solution cannot be considered self-similar. After this stage, the jet cut is performed and the pressure calculation becomes reliable. To verify the cut procedure, three different computations of the water entry of a cone with a deadrise angle $\beta = 30°$ are carried out by using $5°, 10°, 20°$ as limit angles to activate the jet truncation. The corresponding solutions are compared in Fig. 3 in terms of free-surface profiles and pressure distribution along the body. The agreement among the three solutions is rather good, with small differences on the pressure field taking place just behind the jet truncation and about the peak.

An interesting discussion about the effects of numerical models used in the jet region on the local pressure field is reported in Greenhow (1987). In that paper the flow generated during the water entry of a two-dimensional wedge with and without gravity effects is carefully analyzed. In the absence of gravity, when a self-similar solution is expected, negative pressures may occur in the jet region due to artificial constraints applied to keep the jet on the wedge surface. In spite of this unphysical behavior, the overall force on the body is rather insensitive to the details of the flow in the jet region.

In order to check the achievement of a self-similar solution, free-surface profiles and pressure distributions obtained at three different instants of the numerical computation are shown in Fig. 4, where the corresponding asymptotic solution, recovered by Faltinsen and Zhao (1997), is also plotted. To highlight the similarity of the solution, in the graphs spatial variables are scaled by the actual depth of the apex of the cone ζ. The pressure coefficient is defined as

$$C_p = \frac{p}{\frac{1}{2}\rho U^2} .$$

All numerical curves are largely overlapped, thus indicating the representation of a self-similar solution; but they are quite far from the asymptotic solution both in terms of free-surface profile and pressure distribution. These differences

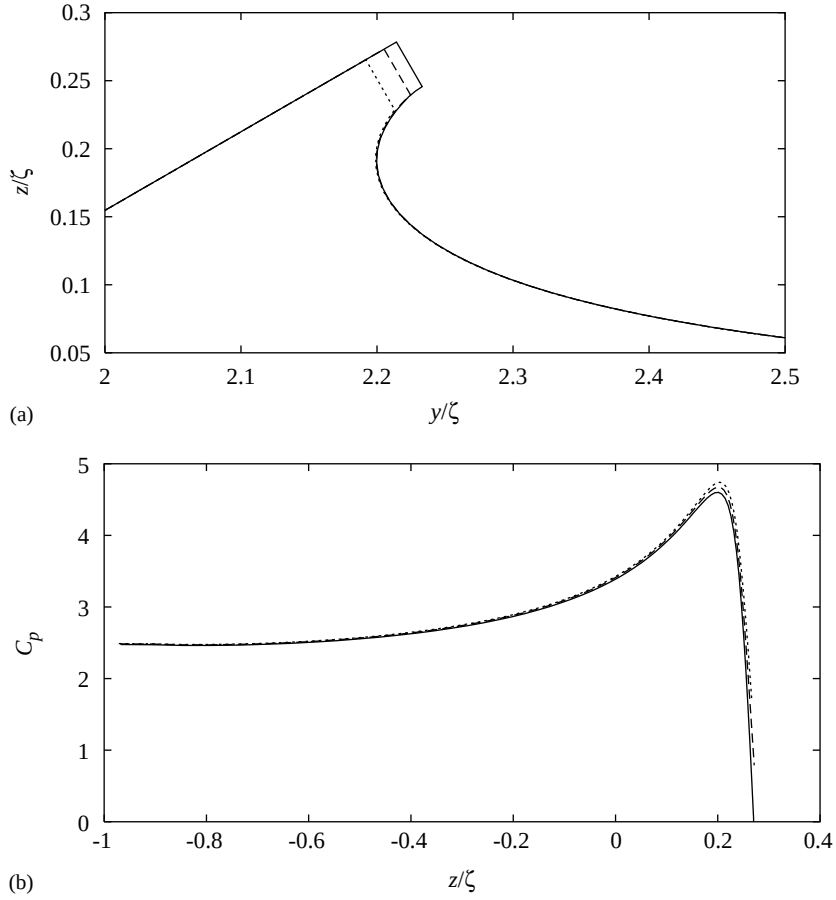

Fig. 3. Solutions obtained for a cone with a deadrise angle $\beta = 30^\circ$ when varying the limit angle used to cut the jet: 5°(——), 10° (----), 20°(···). Results are shown in terms of (a) free-surface elevation and (b) distribution of the pressure coefficient $C_p = p/(\frac{1}{2}\rho U^2)$.

are due to the linearization used in deriving the asymptotic solution, which is no longer valid for such large deadrise angles. Indeed, the same comparison is shown in Fig. 5 for a deadrise angle $\beta = 10^\circ$, and a much better agreement is achieved.

A fully nonlinear theoretical solution for the water impact of a cone with constant entry velocity has been derived by Schiffman and Spencer (1951). Free surface profiles and total hydrodynamic loads have been recovered for the impact with constant entry velocity of a cone with $\beta = 30^\circ$. A zero contact angle between the free surface and the body contour has been assumed in deriving the result.

In Fig. 6 the free-surface profile obtained by using the present numerical model is compared with the solution provided by Schiffman and Spencer (1951) and with that obtained, through the present numerical procedure, for a two-dimensional wedge having the same deadrise angle. The free-surface profile obtained by the present numerical model is in good agreement with the solution by Schiffman and Spencer (1951), although noticeable differences appear close to the jet root. The comparison with the two-dimensional wedge shows the significant reduction in the wetting factor induced by the three dimensionality of the flow.

As a further check of the self-similar solution, the constancy of the arc length between two Lagrangian marker points on the free surface is evaluated (see for example Dobrovol'skaya, 1969; Wagner, 1932). At the beginning, two markers are located on the still free surface and the arc length between them is measured during the motion up to the time when the first Lagrangian point arrives at the jet truncation. In Fig. 7 the position of the arc at several instants of its evolution is shown along with the time history of its length, nondimensionalized by its initial value. Results show that the maximum variation is about 2×10^{-4} of its initial value.

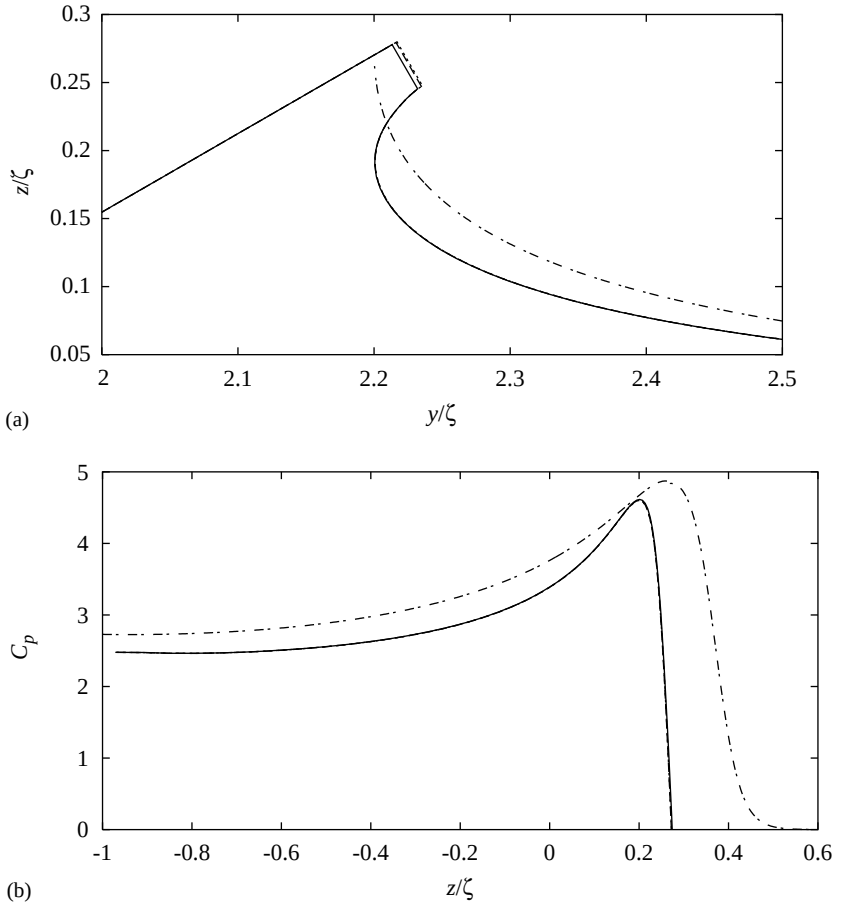

Fig. 4. Check of the self-similarity of the numerical solution obtained for a cone with a deadrise angle $\beta = 30^\circ$. (a) Free-surface configurations and (b) distributions of the pressure coefficient, at $t/t_0 = 4, 8, 12, 16$, where $t_0 = \zeta(0)/U$. The dash–dotted line represents the corresponding asymptotic estimate.

With regard to the total hydrodynamic force, Schiffman and Spencer (1951) give it in the form

$$\frac{F}{\rho} = 3k(\beta)\tan^3(\pi/2 - \beta)U^4\tilde{t}^2, \tag{18}$$

where $\tilde{t}$ is the elapsed time from the instant at which the body touches the free surface and $k(\beta)$ is a nondimensional parameter which depends on the deadrise angle. Three different analytical procedures have been suggested to derive this parameter leading to three estimates with a large scatter among them: $k = 1.44, 1.52, 1.6$. In Schiffman and Spencer (1951) the last value is considered to be the most accurate.

When comparing the numerical solution with the above result, the nonzero initial submergence has to be taken into account. In the present numerical computation, the actual body depth can be written as

$$\zeta = \zeta(0) + Ut = U\tilde{t},$$

that is

$$\tilde{t} = t + \frac{\zeta(0)}{U} = t + t_0.$$

Hence, the total hydrodynamic load is evaluated by integrating the pressure along the body contour, according to Eq. (8), and a least-squares fit is used to present the force in the form

$$\frac{F}{\rho U^4} = c(t + t_0)^2,$$

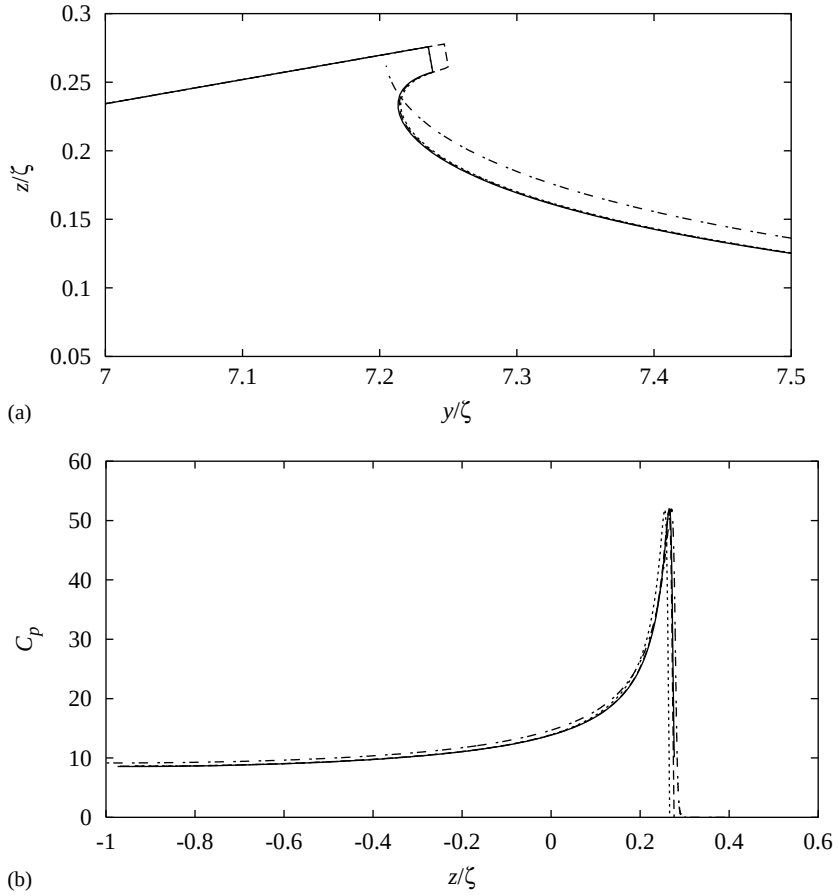

Fig. 5. Check of the self-similarity of the numerical solution obtained for a cone with a deadrise angle $\beta = 10^\circ$. (a) Free-surface configurations and (b) distributions of the pressure coefficient, shown at $t/t_0 = 4, 8, 12, 16$, where $t_0 = \zeta(0)/U$. The dash–dotted line represents the corresponding asymptotic estimate.

which leads to $c = 24.52$. By comparison with Eq. (18), this leads to

$$k = \frac{c}{3\tan^3(\pi/2 - \beta)} = 1.57.$$

This value is in good agreement with the most accurate theoretical prediction, $k = 1.6$, given by Schiffman and Spencer (1951). In Fig. 8a the time histories of the computed hydrodynamic force and of the least-squares fit are compared with that predicted by Eq. (18). In Fig. 8b a close-up view about the origin is shown in terms of the nondimensional time t/t_0, thus revealing that, due to the initial submergence, the extrapolated impact load is nonzero at $t = 0$.

From Fig. 8b some features of the numerical solution during the early stage of the impact can be inferred. Up to $t/t_0 \sim 0.5$ the thin jet is still developing and the computed force is unreliable. Next, a sharp peak appears and, after the first truncation of the jet, the hydrodynamic force starts to decay and approaches the theoretical quadratic trend which is almost completely matched after $t/t_0 \sim 1.5$.

As well as being obtained from the integral of the pressure field through Eq. (8), the total hydrodynamic force can also be evaluated as the time derivative of the kinetic energy which, due to the assumptions made, reads

$$E = -\frac{1}{2}\rho \int_{\partial\Omega} \phi \frac{\partial \phi}{\partial n} \mathrm{d}S.$$

In the numerical calculation, at each time step the kinetic energy of the fluid enclosed into the computational domain is evaluated as

$$E = -\frac{1}{2}\rho \int_{S_B \cup S_F \cup S_T} \phi \frac{\partial \phi}{\partial n} \mathrm{d}S, \tag{19}$$

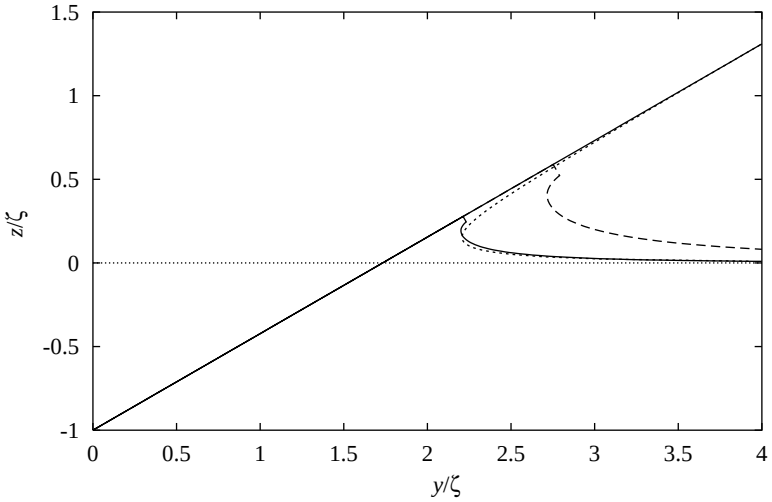

Fig. 6. The free-surface configuration obtained for a cone with a deadrise angle $\beta = 30^\circ$ (——) compared with the fully nonlinear theoretical solution of Schiffman and Spencer (1951) (·····) and with the self-similar solution obtained by using the numerical procedure for a two-dimensional wedge with the same deadrise angle (------).

where S_T denotes the surface of the jet cut and the contribution from S_∞ is omitted owing to the decay properties of the velocity potential. The ratio between the time derivative of the kinetic energy and the hydrodynamic force F, evaluated as the pressure integral (8), is shown in Fig. 9 for the impact of a cone with $\beta = 30^\circ$. The evaluation of the time derivative of the kinetic energy is not computed if a new cut of the jet is made between two successive steps. It can be noticed that, but for the very early stage, the discrepancy is always less than 1% of the computed value.

Due to the cut procedure used to simplify the description of the flow in the jet region, Eq. (19) only provides the part of the kinetic energy which is accumulated in the fluid portion which is within the computational domain. In order to evaluate the part of the kinetic energy which flows into the truncated part of the jet, each time the cut procedure is applied, Eq. (19) is used to compute the kinetic energy in the computational domain before (E_b) and after (E_a) the jet truncation. By summing all the contributions

$$\Delta E_J = E_b - E_a$$

obtained each time a new jet cut is made, the kinetic energy transferred into the truncated part of the jet E_J can be evaluated.

With the aim of understanding which part of the kinetic energy flows into the jet (E_J) and into the bulk of the fluid (E_B), several computations are performed for a two-dimensional wedge and for a cone by varying the deadrise angle. Results, which are reported in Table 1 as a fraction of the total kinetic energy $E_B + E_J$, show that when reducing the deadrise angle the kinetic energy tends to be equally shared between the bulk of the fluid and the jet, as theoretically predicted by Molin et al. (1996). Results also suggest that, for a given deadrise angle, a larger fraction of the kinetic energy flows into the jet in the axisymmetric case compared to the two-dimensional one. It is worth remarking that, due to the model used to cut the jet, the partition of the kinetic energy slightly depends on the limit value of the angle used for the truncation of the jet. However, through some numerical tests, it is found that the inaccuracy in the results reported in Table 1 is less than 2%.

4.2. Circular cylinder

The vertical water entry of a two-dimensional circular cylinder at constant velocity is computed starting from an initial submergence $\zeta(0)/R = 0.00325$. This is a severe test for the numerical procedure, since the local deadrise angle is very small at the beginning and grows during the penetration thus making the cutting procedure really challenging. In the results presented below the limiting angle for the jet cut is fixed at 10°.

Snapshots of three configurations at different stages of the penetration are illustrated in Fig. 10 along with the corresponding distributions of the pressure coefficient. The latter is also compared with that provided by the asymptotic estimate recovered by Cointe and Armand (1987) and also reported in Faltinsen (1990). This asymptotic estimate for

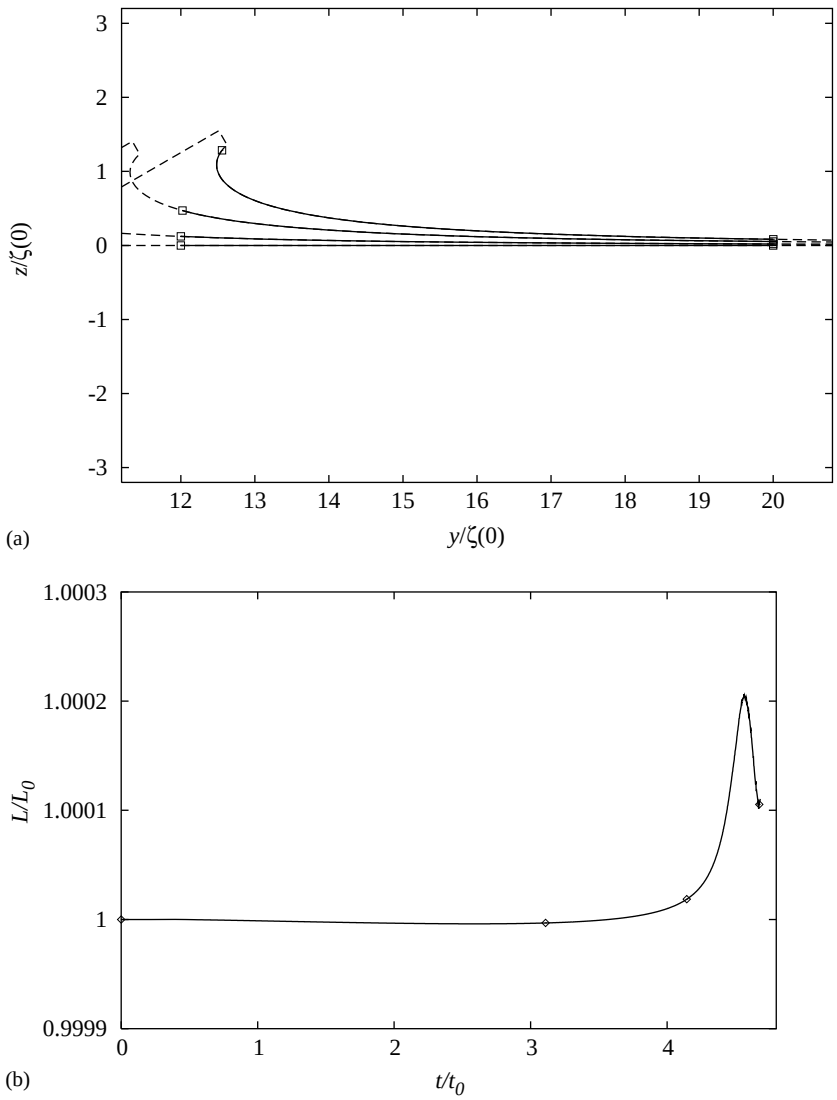

Fig. 7. Check of the constancy of the arc length between two Lagrangian marker points on the free surface ($\beta = 30°$). On (a) the evolution of the arc is shown, on (b) the ratio between the actual length L and its initial value L_0 is shown. Diamonds on picture (b) denote the instants at which the configuration of the arc is plotted on the left-hand side.

the pressure comprises (i) an outer solution, which is singular about the jet root being obtained through the flat plate approximation; and (ii) an evaluation of the maximum pressure peak.

The results in terms of free-surface profiles show that the thickness of the jet grows with the local deadrise angle of the impacting body and that, due to the rise up of the water, the wetted part of the cylinder is significantly larger than the penetration measured at the still water level. The comparison with the asymptotic estimate of the pressure distribution, both in terms of wetted length and of maximum pressure, exhibits a good agreement only during the early stage. Subsequently, the agreement progressively worsens, the asymptotic theory being unable to describe the flow at large deadrise angles.

Regarding the flow features in the jet region, it has to be noted that the growing deadrise angle may result in a detachment of the jet from the body surface even well before the midsection is reached. The question arises as to whether one can check the occurrence of this phenomenon; a first answer could be given by experimental data, if available. As an alternative, in the present calculations the pressure field on the body is monitored: indeed, when the deadrise angle becomes rather large, the artificial constraint which is implicitly introduced by keeping the jet attached to

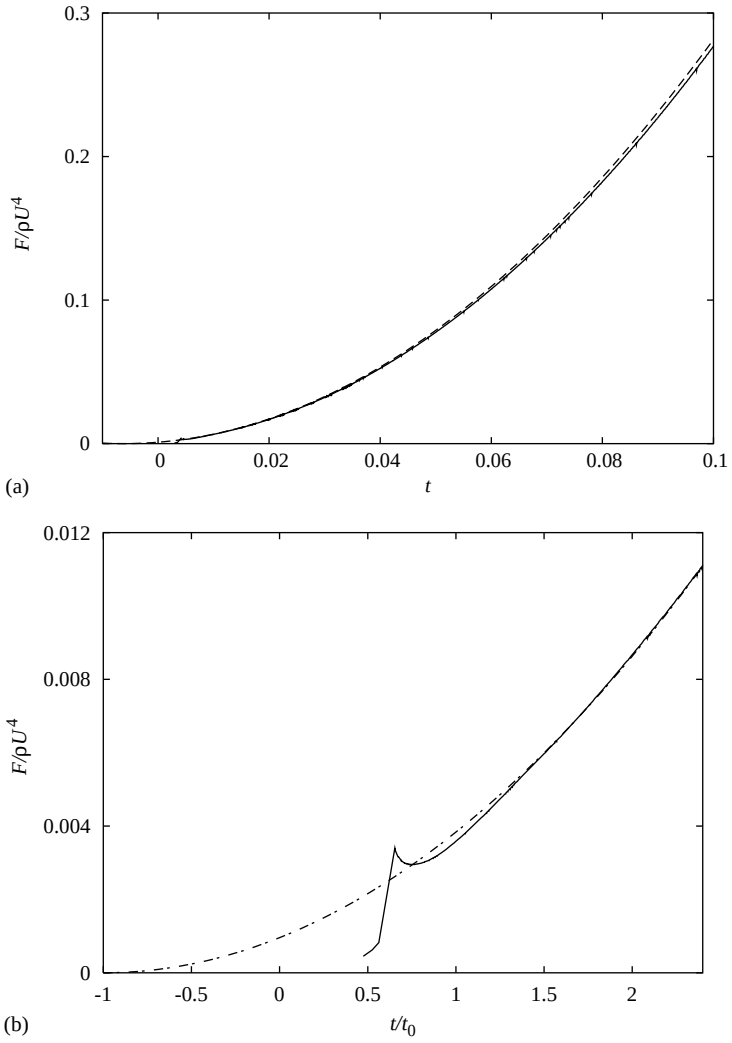

Fig. 8. Time history of the total hydrodynamic force during the impact of a cone with $\beta = 30°$. In (a) the theoretical solution by Schiffman and Spencer (1951) with $k = 1.6$ (-----) and the least-squares fit ($- \cdot - \cdot - \cdot - \cdot -$) are also shown. The fitted curve essentially overlaps the original curve. In (b) the force and the fitted curve are shown in a close-up view around the origin.

the body surface results in a systematic decrease in the amplitude of the (relative) pressure at the jet root (Greenhow, 1987), which eventually becomes negative in a considerable portion of the upper part of the body (Fig. 11 shows the behavior when $\zeta/R = 0.36$). When negative pressure values occur, the adopted numerical model and the corresponding prediction of hydrodynamic force are no longer reliable. In the results obtained here negative pressures in the jet region are found at about $\zeta/R \sim 0.25$.

For validation, numerical results are compared in Fig. 12a with the experimental data provided by Campbell and Weynberg (1980), who performed extensive tests to measure hydrodynamic loads and local pressures. The second-order estimate provided by Cointe and Armand (1987) is also shown. The comparison, in terms of the nondimensional slamming coefficient $C_s = F/\rho U^2 R$, shows that the numerical computation is in good agreement with the experimental data whereas the asymptotic solution, very close to the numerical results at the beginning of the impact, soon starts to overestimate the total hydrodynamic load. A detailed review of several approaches used to evaluate the hydrodynamic loads on an impacting cylinder is provided by Greenhow and Yanbao (1987).

As a verification of the numerical algorithm, the same calculation is carried out by using two more refined discretizations, obtained by successively halving the initial body submergence $\zeta(0)$ and the size of the first panel on the

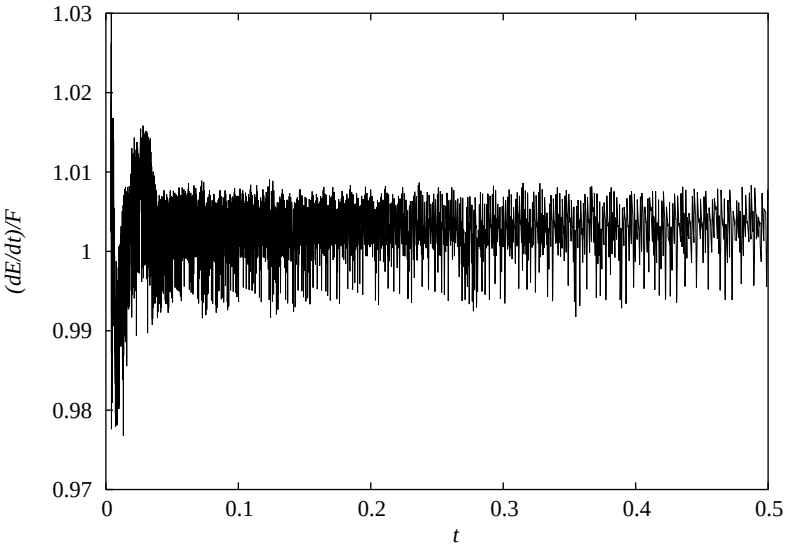

Fig. 9. Time history of the ratio between the time derivative of the kinetic energy E and the hydrodynamic force calculated by means of pressure integration.

Table 1
Kinetic energy partition between the jet and the bulk of the fluid for a two-dimensional wedge and for a cone with different deadrise angles

Deadrise angle	Wedge		Cone	
	$E_B/(E_B+E_J)$	$E_J/(E_B+E_J)$	$E_B/(E_B+E_J)$	$E_J/(E_B+E_J)$
10	0.537	0.463	0.526	0.474
20	0.570	0.430	0.545	0.455
30	0.610	0.390	0.586	0.414
40	0.658	0.342	0.624	0.376
50	0.708	0.292	0.698	0.302

free-surface. The results almost overlap each other, except in a very short region about $\zeta = 0$ for which a close up view is shown in Fig. 12b. By comparing the results, it can be seen that a good agreement is achieved for $\zeta/R > 0.02$. Before that, the computation with the coarser resolution overestimates the total load. This is due to the time the solution needs to adjust, as discussed in the previous section. This delay in approaching the right solution is also responsible for the lack of convergence near the origin. Actually, the use of a more refined resolution makes it possible to anticipate the time at which the solution is reliable, for instance in Fig. 12b the computation with the medium resolution is rather reasonable for $\zeta/R > 0.01$. However, a small initial transient remains during which the solution is still significantly affected by the nonzero initial submergence.

4.3. Sphere

The impact of a rigid sphere of radius R at constant entry velocity is numerically studied. As in the previous case, the initial nondimensional submergence is $\zeta(0)/R = 0.00325$. In Fig. 10a free-surface configurations are shown, and they are compared with the corresponding solution for the circular cylinder. Due to the three-dimensional effect, an evident reduction of the wetted portion of the body contour can be noted. In Fig. 10b, the corresponding pressure distributions are also depicted and compared with the asymptotic estimate provided by Faltinsen and Zhao (1997). As for the cylinder case, numerical results are in good agreement with the asymptotic theory only during the initial stage of the impact. Later, as aforementioned, due to the increased deadrise angle, the asymptotic solution is unable to provide a

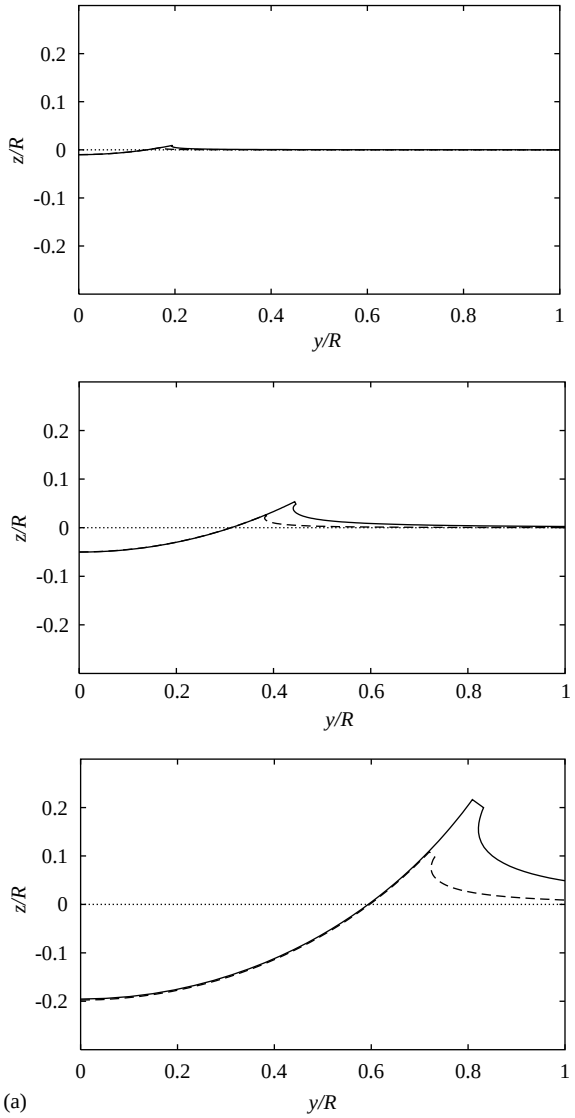

Fig. 10. Comparison between the impact of a two-dimensional circular cylinder and a sphere. (a) Free-surface configurations are shown for the impact of a circular cylinder (—) and of a sphere (- - - - - -) at three different penetration stages: $\zeta/R = 0.01$ (a), 0.05, 0.2. (b) Pressure fields at the same penetration stages: cylinder, present method (——) and asymptotic solution (- - - - - and □); sphere, present method (· · · · · ·) and asymptotic solution (– · – · – · – · –).

good estimate. Due to the three-dimensional effect, a reduction in the overall pressure distribution is also observed. As for the circular cylinder, the occurrence of negative pressures resulting in jet flow separation is monitored: in this case the pressure becomes definitely negative in the jet region at about $\zeta/R \sim 0.43$.

The total slamming coefficient $C_s = F/0.5\rho\pi R^2 U^2$ is calculated from pressure integration and plotted versus ζ/R in Fig. 13, along with the slamming coefficient given by the asymptotic estimate. Unlike the case of the cylinder, the hydrodynamic load on the sphere does not have an impulsive character, but it starts from zero, quickly rises up to the maximum and then smoothly decays (Miloh, 1981). The numerical results are compared with experimental data provided by Baldwin and Steves (1975) and with the data by Nisewanger (1961), also reported in Wardlaw and Aronson (1977). The agreement is quite satisfactory throughout the considered interval. As expected the asymptotic estimate largely overpredicts the slamming coefficient after $\zeta/R = 0.05$.

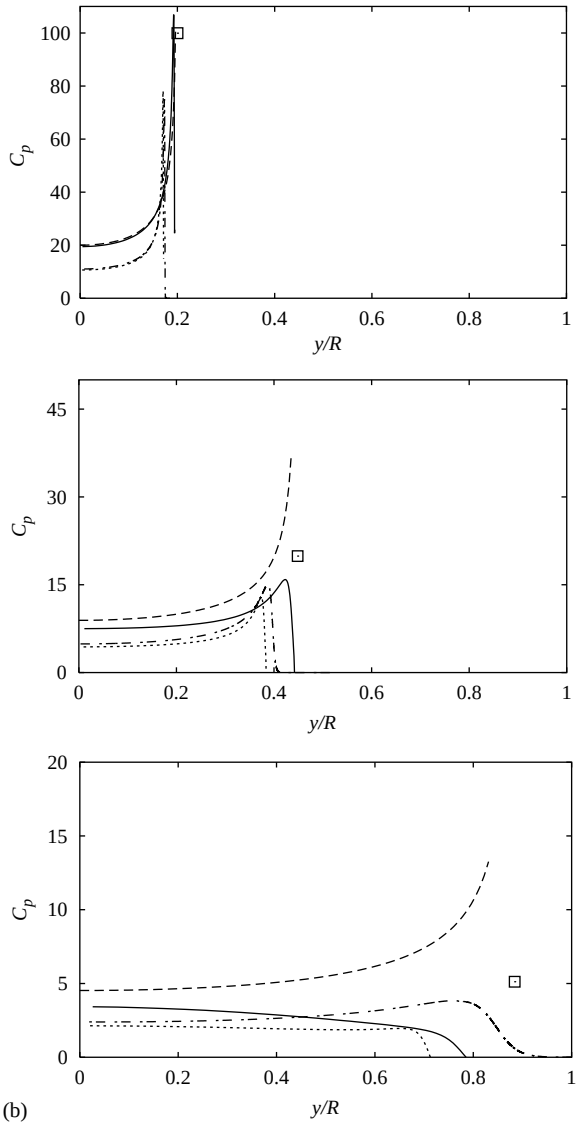

(b)

Fig. 10 (*continued*).

Beside those studies aforementioned, Moghisi and Squire (1981) also performed an extensive series of tests, and summarized the impact load results in a best fit curve, valid for submergence $\zeta/R<0.18$. Following their representation, in Fig. 13b several curves describing the reduced coefficient $C_s/\sqrt{\zeta/R}$ versus the reduced nondimensional submergence $\sqrt{\zeta/R}<0.42$ are plotted. In this representation, the early stage experimental results by Baldwin and Steves (1975) and Nisewanger (1961) exhibit a rather pronounced scatter, probably due to the difficulties in carrying out measurements in the very initial transient.

The comparison of the numerical results with the experimental data reported in Moghisi and Squire (1981) and with the theoretical estimate provided by Miloh (1991) and Faltinsen and Zhao (1997) is not satisfactory. Regarding the behavior of the slamming coefficient for small times predicted by asymptotic theories, Faltinsen and Zhao (1997) and Miloh (1981) showed that, at leading order for small ζ/R, C_s behaves like

$$C_s = A_0(\zeta/R)^{1/2} + \mathcal{O}(\zeta/R),$$

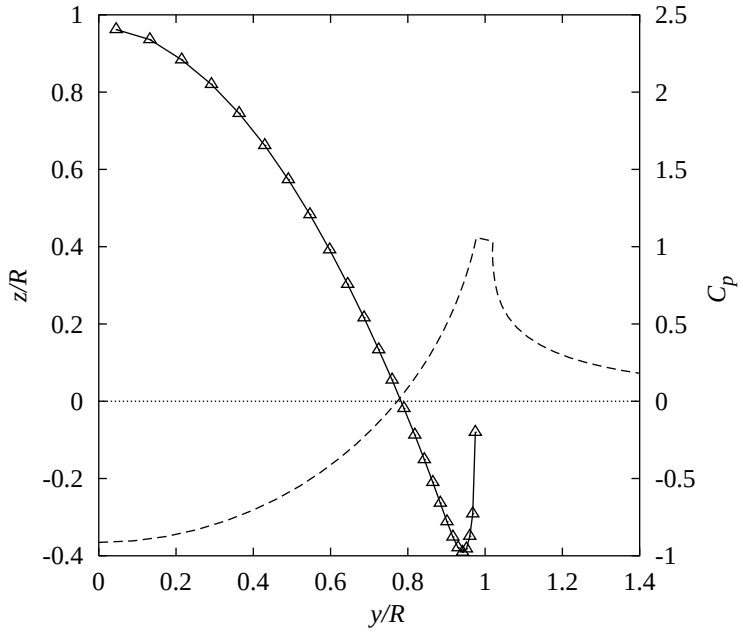

Fig. 11. Free-surface configuration (– – –) and pressure distribution (—△—) for the impact of a circular cylinder at $\zeta/R = 0.36$. The occurrence of negative pressures in the jet region is evident for $y/R > 0.8$.

where $A_0 = 12\sqrt{3}/\pi = 6.61$. Through a different assumption on the wetted correction, in Miloh (1991) the estimate $A_0 = 5.50$ has been used, and this may be the reason for the difference between the two theoretical solutions about $\zeta = 0$ (Fig. 13b).

As a further validation of the unsteady calculation, the time histories of the pressure field at two circumferential positions are extracted from the numerical solution and compared in Fig. 14 with those experimentally measured by Nisewanger (1961), showing a rather satisfactory agreement.

Before closing this section it is worth remarking that, due to the flatness of the impacting geometry, in the very early stage of the impact the present numerical model is not really appropriate in correctly describing the phenomenon, since compressibility and air cushion effects are then relevant (Korobkin and Pukhnachov, 1988).

5. Final remarks

In the present paper the water impact of two-dimensional and axisymmetric bodies have been investigated with attention mainly focused on the analysis of the resulting hydrodynamic loads. The study has been carried out by using a numerical approach based on a fully nonlinear boundary-element method, which uses a suitable model to describe the jet flow that originates at the intersection of the body contour and the free surface due to the local flow singularity. The water impact with constant entry velocity of a cone, of a circular cylinder and of a sphere has been analyzed, and comparisons have been established with existing theoretical and experimental results. The approach has been found to be rather stable and reliable after a short initial transient phase. Future work is planned to extend the jet modeling to the case of flow separation, thus allowing the model to be also applicable to convex bodies with rather sharp variation of the deadrise angle.

Acknowledgements

This work was supported by the *Ministero delle Infrastrutture e dei Trasporti* in the framework of INSEAN research plan 2000–2002.

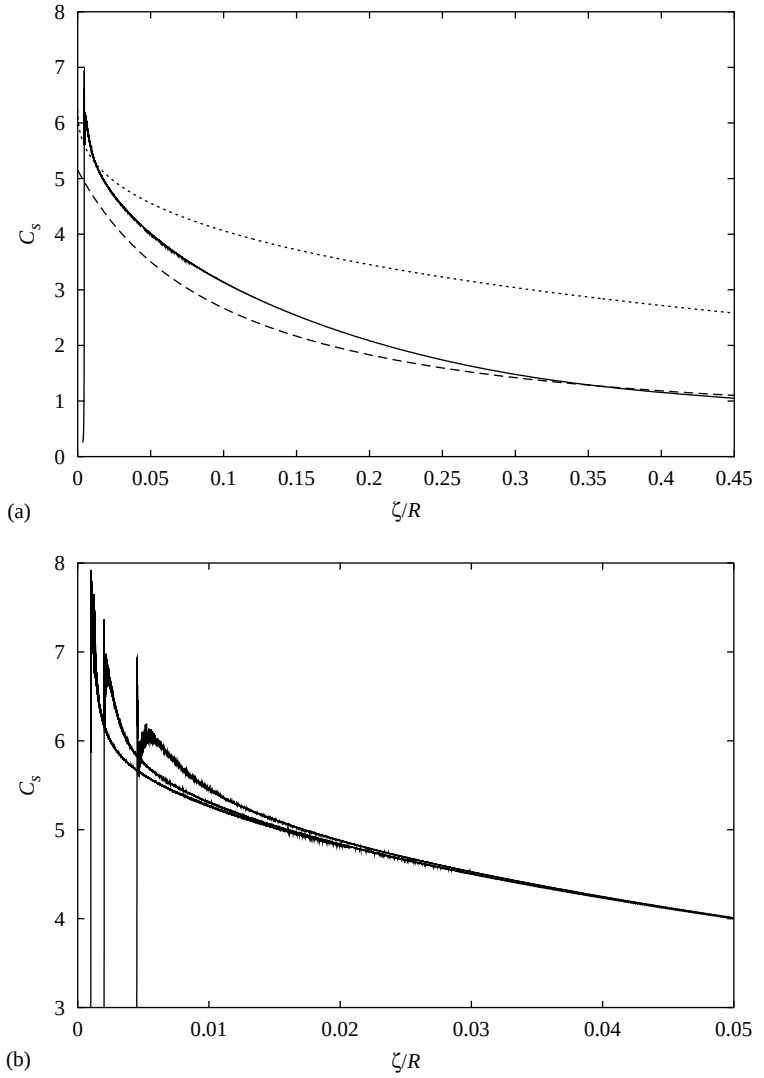

Fig. 12. Slamming coefficient $C_s = F/\rho R U^2$ versus the nondimensional submergence ζ/R for the impact of a cylinder. (a) The numerical results (—) are compared with experimental data by Campbell and Weynberg (1980) (------) and with the second-order asymptotic solution by Cointe and Armand (1987) ($\cdot\cdot\cdot\cdot$). (b) The comparison of numerical results obtained with three different discretizations during the early stage of the simulations.

Appendix A. Reduction of $\boldsymbol{n}\cdot(\boldsymbol{w}\cdot\nabla)\boldsymbol{u}$

Let a generic point P of an axisymmetric surface be identified by

$$\boldsymbol{x}_P(\xi_1,\xi_2) = (x_P, y_P, z_P) = (r(\xi_2)\cos\xi_1, r(\xi_2)\sin\xi_1, z(\xi_2)), \tag{A.1}$$

where ξ_2 is the curvilinear abscissa along the meridian contour, and ξ_1 is the azimuthal angle. If ξ_2 is the natural parameter, the relation $|\partial\boldsymbol{x}_P/\partial\xi_2|^2 = r'^2 + z'^2 = 1$ holds, where prime denotes the differentiation with respect to ξ_2. In the following, partial differentiation is abbreviated as $\partial_i \equiv \partial/\partial\xi_i$ and summation over repeated symbols is implicitly assumed; Latin indices range over $1,2,3$, whereas Greek ones range over $1,2$.

At P a frame of reference $\{\boldsymbol{s}_1,\boldsymbol{s}_2,\boldsymbol{s}_3\}$ can be introduced as follows:

$$\boldsymbol{s}_1 = \frac{\partial\boldsymbol{x}_P}{\partial\xi_1}, \quad \boldsymbol{s}_2 = \frac{\partial\boldsymbol{x}_P}{\partial\xi_2}, \quad \boldsymbol{s}_3 = \boldsymbol{n} = \frac{\boldsymbol{s}_1\times\boldsymbol{s}_2}{|\boldsymbol{s}_1\times\boldsymbol{s}_2|}, \tag{A.2}$$

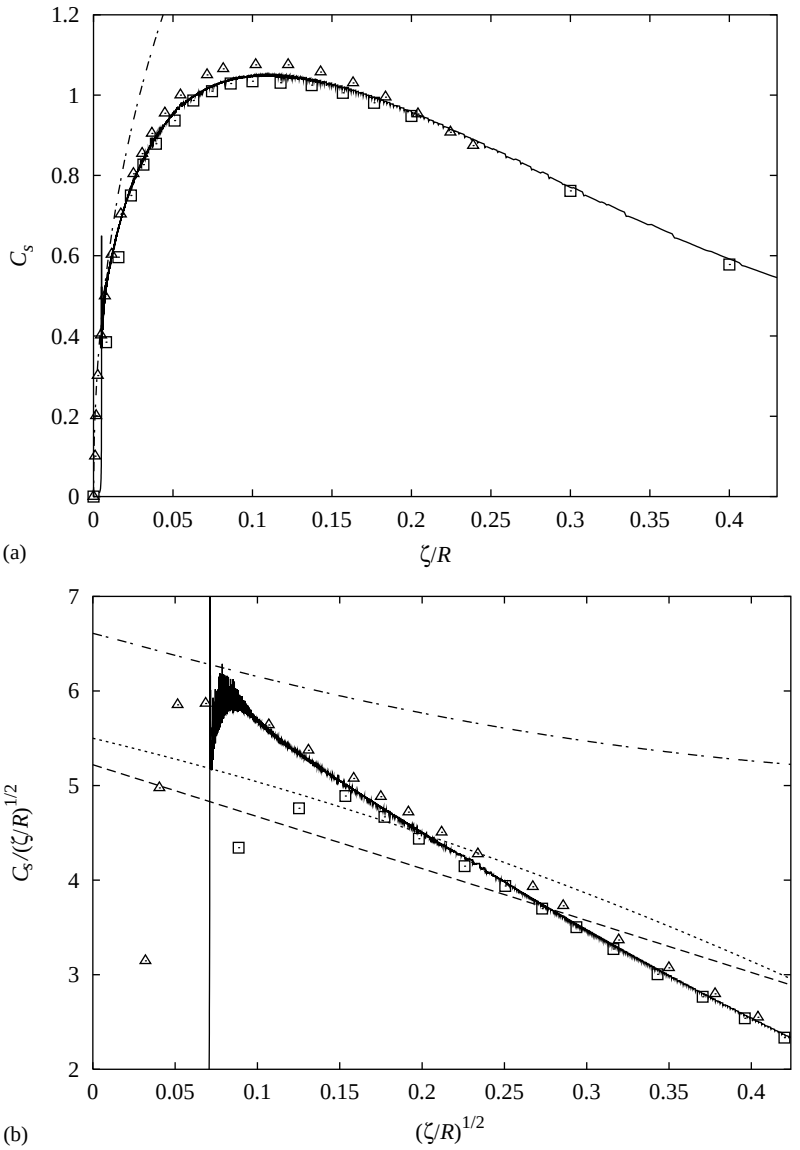

Fig. 13. Slamming coefficient $C_s = F/0.5\rho\pi R^2 U^2$ versus the nondimensional submergence for the impact of a sphere. (a) Numerical results (——) are compared with experimental data by Baldwin et al. (1975) (□) and by Nisewanger (1961) (△) and with asymptotic solution (– · – · – · – · –). (b) The reduced slamming coefficient $C_s/\sqrt{\zeta/R}$ versus $\sqrt{\zeta/R}$. Numerical results (——) are compared with experimental data by Baldwin and Steves (1975) (□), by Nisewanger (1961) (△), and by Moghisi and Squire (1981) (– – – – –). The theoretical estimate by Miloh (1991) (· · · · ·) and the asymptotic solution by Faltinsen and Zhao (1997) (– · – · – · – · –) are also shown.

which is orthogonal but not orthonormal. Dealing with a curved surface and with a local nonorthonormal basis, it is useful to adopt the formalism of a generic curved surface embedded in an Euclidean three-dimensional space. As a first step, the components of the metric tensor $g_{ij} = \boldsymbol{s}_i \cdot \boldsymbol{s}_j$ are calculated, giving $g_{11} = 1/g^{11} = r^2$, $g_{22} = g^{22} = 1$, $g_{33} = g^{33} = 1$. From the metric tensor components it is evident that the second and third contravariant components a^2, a^3 of a generic vector $\boldsymbol{a} = a^i \boldsymbol{s}_i$ coincide with their covariant counterparts a_2, a_3.

The continuity equation in curvilinear coordinates reads $\nabla_i u^i = g^{ij}\nabla_i u_j = 0$, where ∇_i is the covariant derivative; that for a covariant vector a_i provides

$$\nabla_i a_j = \partial_i a_j - \Gamma_{ij}^k a_k,$$

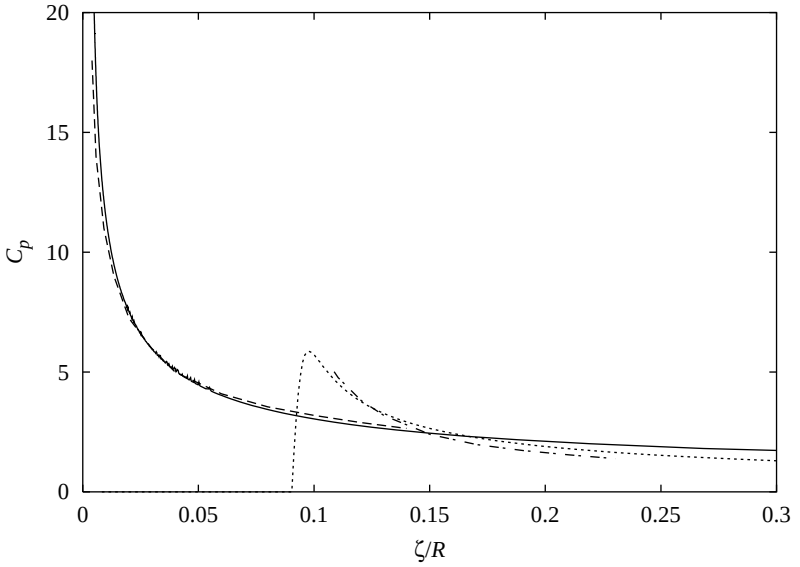

Fig. 14. Pressure histories at fixed circumferential locations (0° and 30°) for the impact of a sphere. Numerical results (0°, ——; 30°, · · · · ·) and experimental data by Nisewanger (1961) (0°, – – – – – – –; and 30° (– · – · – · – · –)).

Γ^k_{ij} being the Christoffel symbols, $\Gamma^k_{ij} = g^{kl}\Gamma_{ijl} = g^{kl}(\boldsymbol{s}_l \cdot \partial_i \boldsymbol{s}_j) = g^{kl}(\boldsymbol{s}_l \cdot \partial_j \boldsymbol{s}_i)$. In particular, it follows that (Flügge, 1972):

$$\Gamma^\alpha_{33} = \Gamma^3_{3\alpha} = \Gamma^3_{\alpha 3} = 0 \tag{A.3}$$

and

$$\Gamma^3_{\alpha\beta} = \Gamma_{\alpha\beta 3} = -\Gamma_{\alpha 3\beta} = b_{\alpha\beta}, \quad \alpha, \beta = 1, 2, \tag{A.4}$$

where $b_{\alpha\beta} = \boldsymbol{n} \cdot \partial_\alpha \partial_\beta \boldsymbol{x}_P$ is the *second fundamental quadratic form* of the surface. By exploiting the axisymmetric and swirl-free hypotheses it follows that $u_1 = \partial_1 u_1 = 0$, and then the continuity equation provides

$$\partial_3 u_3 = \nabla_3 u_3 = -\partial_2 u_2 + g^{ij}\Gamma^k_{ij} u_k = -\partial_2 u_2 + g^{11}\Gamma^2_{11} u_2 + \Gamma^2_{22} u_2 + g^{11} b_{11} u_3 + b_{22} u_3. \tag{A.5}$$

By using the above relation and again the axisymmetric swirl-free hypotheses, the term $\boldsymbol{n} \cdot (\boldsymbol{w} \cdot \nabla)\boldsymbol{u}$ is rearranged as follows:

$$\begin{aligned} \boldsymbol{n} \cdot (\boldsymbol{w} \cdot \boldsymbol{\nabla})\boldsymbol{u} &= w^j \nabla_j u_3 = w^2 \nabla_2 u_3 + w^3 \nabla_3 u_3 = w^2(\partial_2 u_3 - \Gamma^2_{23} u_2) + w^3 \nabla_3 u_3 \\ &= w^2(\partial_2 u_3 + b_{22} u_2) + w^3(-\partial_2 u_2 + g^{11}\Gamma^2_{11} u_2 + \Gamma^2_{22} u_2 + g^{11} b_{11} u_3 + b_{22} u_3). \end{aligned} \tag{A.6}$$

In Eq. (A.6) only two Christoffel symbols appear $\Gamma^2_{11} = \boldsymbol{s}_2 \cdot \partial_1 \boldsymbol{s}_1$ and $\Gamma^2_{22} = \boldsymbol{s}_2 \cdot \partial_2 \boldsymbol{s}_2$, that can be calculated by differentiating equation (A.1) twice, thus obtaining

$$\Gamma^2_{11} = -rr', \quad \Gamma^2_{22} = 0. \tag{A.7}$$

For a generic curve lying on the surface the following relation holds (Dubrovin et al., 1986):

$$k \cos\theta = \frac{b_{\alpha\beta}\, \mathrm{d}\xi^\alpha\, \mathrm{d}\xi^\beta}{g_{\alpha\beta}\, \mathrm{d}\xi^\alpha\, \mathrm{d}\xi^\beta}, \quad \alpha, \beta = 1, 2, \tag{A.8}$$

where k is the local curvature and θ is the angle between the normal to the curve and the normal to the surface with $k\cos\theta$ therefore being the normal curvature k_n (taken with its sign) of the considered curve. For the two coordinate lines $\boldsymbol{\gamma}_1(\xi_1) = \boldsymbol{x}_P(\xi_1, \xi_2 = cost)$ and $\boldsymbol{\gamma}_2(\xi_2) = \boldsymbol{x}_P(\xi_1 = cost, \xi_2)$, Eq. (A.8) gives

$$k_{1n} = b_{11}/g_{11} = b_{11} g^{11}, \quad k_{2n} = b_{22}/g_{22} = b_{22}, \tag{A.9}$$

respectively. By using Eqs. (A.9) and (A.7) and the explicit form of the metric tensor g_{ij}, relation (A.6) provides (Battistin and Iafrati, 2001)

$$\boldsymbol{n} \cdot (\boldsymbol{w} \cdot \boldsymbol{\nabla})\boldsymbol{u} = w_2 \partial_2 u_3 - w_3 \partial_2 u_2 + k_{2n} w_2 u_2 + (k_{1n} + k_{2n}) w_3 u_3 - \frac{r'}{r} w_3 u_2. \tag{A.10}$$

The two-dimensional expression is recovered by simply neglecting, in Eq. (A.6), the contributions related to the azimuthal parameter ξ_1:

$$\boldsymbol{n}\cdot(\boldsymbol{w}\cdot\boldsymbol{\nabla})\boldsymbol{u} = w_2\partial_2 u_3 - w_3\partial_2 u_2 + k_2\boldsymbol{w}\cdot\boldsymbol{u}. \tag{A.11}$$

In Eqs. (13) and (14), ξ_1 and ξ_2 are replaced by θ and s, respectively.

References

Baldwin, L., Steves, H.X., 1975. Vertical water entry of spheres. NSWC/WOL/TR 75-49, White Oax Laboratory, Silver Spring, MD, USA.

Battistin, D., Iafrati, A., 2001. Water impact of 2D and axisymmetric bodies of arbitrary section. INSEAN Technical Report No. 06/01, Roma.

Campbell, I.M.C., Weynberg, P.A., 1980. Measurement of parameters affecting slamming. Report No 440, Wolfson Unit of Marine Technology, Tech. Rep. Centre No. OT-R-8042, Southampton, UK.

Cointe, R., 1989. Nonlinear simulation of transient free surface flows. Proceedings of the Fifth International Conference on Numerical Ship Hydrodynamics, Hiroshima, Japan.

Cointe, R., Armand, J.L., 1987. Hydrodynamic impact analysis of a cylinder. ASME Journal of Offshore Mechanics and Arctic Engineering 109, 237–243.

Dobrovol'skaya, Z.N., 1969. On some problems of similarity flow of fluid with a free-surface. Journal of Fluid Mechanics 36, 805–829.

Dubrovin, B.A., Novikov, S.P., Fomenko, A.T., 1986. Geometria delle superfici, dei gruppi di trasformazione e dei campi. Vol I. Ed. Riuniti. Italian translation of Sovremennaja geometrija. Metody i priloženija, Nauka, Moscow (Russia).

Faltinsen, O.M., 1990. Sea Loads on Ships and Offshore Structures. Cambridge University Press, Cambridge.

Faltinsen, O.M., Zhao, R., 1997. Water entry of ship sections and axisymmetric bodies. Proceedings of AGARD FDP Workshop on High speed Body Motion in Water, Kiev, Ukraine.

Faltinsen, O.M., Rognebakke, O.F., Lukovsky, A.J., Timoka, A.M., 1999. Multidimensional modal analysis of non-linear sloshing in a rectangular tank with finite depth. Journal of Fluid Mechanics 407, 201–211.

Flügge, W., 1972. Tensor Analysis and Continuum Mechanics. Springer, New York.

Fontaine, E., Cointe, R., 1997. Asymptotic theories of incompressible water entry. Proceedings of AGARD FDP Workshop on High Speed Body Motion in Water, Kiev, Ukraine.

Gradshteyn, I.S., Ryzhik, I.M., 1980. Table of Integrals, Series and Products. Academic Press, London.

Greenhow, M., 1987. Wedge entry into initially calm water. Applied Ocean Research 9, 214–223.

Greenhow, M., 1988. Water-entry and -exit of a circular cylinder. Applied Ocean Research 10, 191–198.

Greenhow, M., Yanbao, L., 1987. Added masses for circular cylinders near or penetrating fluid boundaries-review, extension and application to water-entry, -exit and slamming. Ocean Engineering 14, 325–348.

Iafrati, A., Korobkin, A.A., 2001. Starting flow generated by a floating wedge impact. Proceedings of the 16th International Workshop on Water Waves and Floating Bodies, Hiroshima, Japan.

Iafrati, A., Carcaterra, A., Ciappi, E., Campana, E.F., 2000. Hydroelastic analysis of a simple oscillator impacting the free surface. Journal of Ship Research 44, 278–289.

Korobkin, A.A., Pukhnachov, V.V., 1988. Initial stage of water impact. Annual Review of Fluid Mechanics 20, 159–185.

Longuet-Higgins, M.S., Cokelet, E.D., 1976. The deformation of steep surface waves on water. I. A numerical method. Proceedings of the Royal Society, London A 350, 1–26.

Miloh, T., 1981. Wave slam on a sphere penetrating a free-surface. Journal of Engineering Mathematics 15, 221–240.

Miloh, T., 1991. On the initial-stage slamming of a rigid sphere in a vertical entry. Applied Ocean Research 13, 43–48.

Moghisi, M., Squire, P.T., 1981. An experimental investigation of the initial force of impact on a sphere striking a liquid surface. Journal of Fluid Mechanics 108, 133–146.

Molin, B., Cointe, R., Fontaine, E., 1996. On energy arguments applied to slamming force. Proceedings of the 11th International Workshop of Water Waves and Floating Bodies, Hamburg, Germany.

Nisewanger, C.R., 1961. Experimental determination of pressure distribution on a sphere during water entry. NAVWEPS Rep. No. 7808.

Savander, B.R., 1997. Planing hull steady hydrodynamics. Ph.D. Thesis, Department of Naval Architecture and Marine Engineering, University of Michigan, USA.

Schiffman, M., Spencer, D.C., 1951. The force of impact on a cone striking a water surface (vertical entry). Communications on Pure and Applied Mathematics 4, 379–417.

Tanizawa, K., 1995. A nonlinear simulation method of 3-D body motion in waves—1st report. Journal of the Society of Naval Architects of Japan 178, 179–191.

Wagner, H., 1932. Über stoß- und Gleitvorgänge an der Oberfläche von Flüssigkeiten. Zeitschrift fr Angewandte Mathematik und Mechanik, 12, 192–215.

Wardlaw, A.B. Jr., Aronson, P.M., 1977. Prediction of surface pressure during water impact. N77-23410, Lincoln Lab., Massachussetts Institute of Technology, Cambridge, MA, USA.

Wu, G.X., Eatock Taylor, R., 1996. Transient Motion of a floating body in steep water waves. Proceedings of the 11th International Workshop on Water Waves and Floating Bodies, Hamburg, Germany.

Xu, L., Troesh, A.W., 1999. A study on hydrodynamics of asymmetric planing surfaces. Proceedings of FAST '99 Conference, Seattle, USA, pp. 471–481.

Zhao, R., Faltinsen, O.M., 1993. Water entry of two-dimensional bodies. Journal of Fluid Mechanics 246, 593–612.

Zhao, R., Faltinsen, O.M., Aarnes, J., 1996. Water entry of arbitrary two-dimensional sections with and without flow separation. Proceedings of the 21st International Symposium on Naval Hydrodynamics, Trondheim, Norway, pp. 118–132.

Zhao, R., Faltinsen, O.M., Haslum, H.A., 1997. A simplified nonlinear analysis of a high speed planing craft in calm water. Proceedings of FAST '97 Conference, Sydney, Australia, pp. 431–438.